

PL-TR-92-2305

AD-A263 209



**CRUSTAL AND UPPER MANTLE VELOCITY GRADIENTS
IN THE VICINITY OF THE EAST KAZAKH TEST SITE;
RAY SYNTHESIS OF L_g IN THREE DIMENSIONAL
CRUSTAL MODELS**

Vernon F. Cormier
Michael D. Kalmbach
Henjie Zhao

University of Connecticut
Department of Geology and Geophysics
Storrs, CT 06269-2045

30 October 1992

Final Report
1 September 1990-19 October 1992



Approved for public release; distribution unlimited



PHILLIPS LABORATORY
Directorate of Geophysics
AIR FORCE MATERIEL COMMAND
HANSCOM AIR FORCE BASE, MA 01731-5000

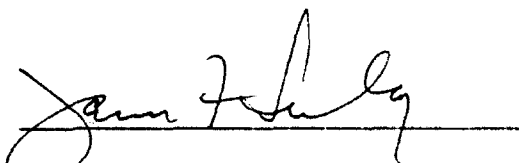
93-08573



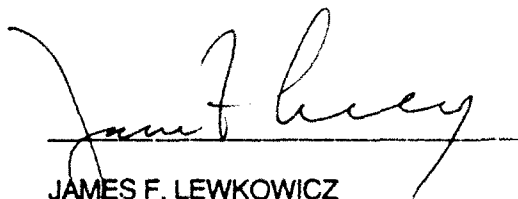
39-261

The views and conclusions contained in this document are those of the authors and should not be interpreted as representing the official policies, either expressed or implied, of the Air Force or the U.S. Government.


This technical report has been reviewed and is approved for publication.



JAMES F. LEWKOWICZ
Contract Manager
Solid Earth Geophysics Branch
Earth Sciences Division



JAMES F. LEWKOWICZ
Branch Chief
Solid Earth Geophysics Branch
Earth Sciences Division


DONALD H. ECKHARDT, Director
Earth Sciences Division

This document has been reviewed by the ESD Public Affairs Office (PA) and is releasable to the National Technical Information Service (NTIS).

Qualified requestors may obtain additional copies from the Defense Technical Information Center. All others should apply to the National Technical Information Service.

If your address has changed, or if you wish to be removed from the mailing list, or if the addressee is no longer employed by your organization, please notify PL/IMA, Hanscom AFB MA 01731-5000. This will assist us in maintaining a current mailing list.

Do not return copies of this report unless contractual obligations or notices on a specific document requires that it be returned.

REPORT DOCUMENTATION PAGE			Form Approved OMB No. 0704-0188	
<small>Public reporting burden for this collection of information is estimated to average 1 hour per response, including the time for reviewing instructions, searching existing data sources, gathering and maintaining the data needed, and completing and reviewing the collection of information. Send comments regarding this burden estimate or any other aspect of this collection of information, including suggestions for reducing this burden, to Washington Headquarters Services, Directorate for Information Operations and Reports, 1215 Jefferson Davis Highway, Suite 1204, Arlington, VA 22202-4302, and to the Office of Management and Budget, Paperwork Reduction Project (0704-0188), Washington, DC 20503</small>				
1. AGENCY USE ONLY (Leave blank)		2. REPORT DATE 30 October 1992		3. REPORT TYPE AND DATES COVERED Final (1 Sep 1990-19 Oct 1992)
4. TITLE AND SUBTITLE Crustal and Upper Mantle Velocity Gradients in the Vicinity of the East Kazakh Test Site; Ray Synthesis of Lg in Three-Dimensional Crustal Models			5. FUNDING NUMBERS PE 62101F PR 7600 TA 09 WU AW Contract F19628-90-K-0043	
6. AUTHOR(S) Vernon F. Cormier Michael D. Kalmbach Hanjie Zhao				
7. PERFORMING ORGANIZATION NAME(S) AND ADDRESS(ES) University of Connecticut Department of Geology and Geophysics Storrs, CT 06269-2045			8. PERFORMING ORGANIZATION REPORT NUMBER	
9. SPONSORING/MONITORING AGENCY NAME(S) AND ADDRESS(ES) Phillips Laboratory Hanscom AFB, MA 01731-5000 Contract Manager: James Lewkowicz/GPEH			10. SPONSORING/MONITORING AGENCY REPORT NUMBER PL-TR-92-2305	
11. SUPPLEMENTARY NOTES				
12a. DISTRIBUTION/AVAILABILITY STATEMENT Approved for public release: distribution unlimited			12b. DISTRIBUTION CODE	
13. ABSTRACT (Maximum 200 words) Using a simple homogeneous crust and a first order Moho discontinuity, Lg waveforms are synthesized in canonical models as well as models chosen for selected Eurasian paths. Lg blockage by basins and Moho transitions is a strong function of the slope of the Moho surface and is only a weak function of the angle of source-receiver path relative to the strike of the structure. Synthetic waveforms are often in good qualitative agreement with observed waveforms, including details in the shape of the Lg coda. Poorer agreement is seen in cases in which either (a) the inferred Moho from surface topography disagrees with that determined from deep seismic sounding observations or (b) sedimentary basin structure is not included in the synthetic modeling. Synthetics that allow single scattering incorporated by the Born approximation show that scattering by heterogeneity within the crustal waveguide can fill up the Lg coda between multiple SmS arrivals and lengthen the Lg coda. The trajectories and geometric spreading of rays contributing to Lg suggest that the most important effects of scattering will be concentrated in the Moho transition and in the upper several kilometers of the crust.				
14. SUBJECT TERMS Lg, synthetic seismograms, crustal structure			15. NUMBER OF PAGES 30	
			16. PRICE CODE	
17. SECURITY CLASSIFICATION OF REPORT Unclassified	18. SECURITY CLASSIFICATION OF THIS PAGE Unclassified	19. SECURITY CLASSIFICATION OF ABSTRACT Unclassified	20. LIMITATION OF ABSTRACT SAR	

Table of Contents

INTRODUCTION.....	1
RESULTS	
Propagation Perpendicular to a Mountain Range.....	1
Propagation Parallel to a Mountain Range.....	2
Propagation Oblique to a Mountain Range.....	2
Width of Crustal Transition.....	3
Propagation Across the Tibet Plateau.....	3
Scattering Within the Crustal Waveguide.....	4
Importance of Scattering in Different Depth Regions of the Crust.....	5
CONCLUSIONS AND RECOMMENDATIONS	
Modeling Results.....	5
Lessons Learned from Ray Based Approaches to Regional Seismogram Synthesis....	6
FIGURES.....	7
REFERENCES.....	17

DTIC QUALITY CONTROL
iii

For	
SI	<input checked="" type="checkbox"/>
Unannounced Justification	<input type="checkbox"/>
By	
Distribution/	
Availability Codes	
Dist	Special and/or Special
A-1	

INTRODUCTION

In this report we summarize the results of experiments in which Lg waveforms are synthesized either by dynamic raytracing and or superposition of Gaussian beams (Červený, 1985) in three-dimensionally varying crustal waveguides. In both approaches, Lg is represented as a sum of multiply critically reflected SmS waves (Figure 1). Topography of the Moho is correlated with given, or known surface topography under the assumption of Airy isostasy. The starting assumptions are essentially the same as those used by Kennett (1986) in identifying gross effects of crustal thickness on Lg by plotting the bounce points of critically reflected S waves in the crust. Here, however, waveforms are calculated and the effects of geometric spreading are included. Details of the modeling approach, including source functions assumed, are described in (Cormier and Kalnay, 1991).

RESULTS

Propagation Perpendicular to a Mountain Range

Lg is modeled by summing dynamically traced rays in a laterally varying crustal waveguide simulating a hypothetical mountain range. Crustal thickness contours are shown in map view in Figure 1a. Certain characteristics, such as the square corners of the contour lines, are concessions made for modeling simplicity and are not expected to greatly influence the results. Background crustal thickness is taken as 35 km, which represents continental crust slightly elevated above sea level. The thickness of the mountain root is 50 km, which is consistent with gravity surveys in various high mountainous regions (e.g. Press and Siever, 1982, p. 437). A physical analogy to this model may be found in the South American Andes, which is similarly a narrow range with abrupt fronts on both sides.

Tested propagation paths are shown in Figure 1a and ray synthetic seismograms in Figure 1b for a vertical point force. The first trace shows Lg at the same offset as receiver R_1 through an undisturbed waveguide. Traces 2 through 4 are recordings from receiver locations R_1 through R_4 . Visual comparison of the traces gives a measure of attenuation and the extensive numerical data from the program runs explain the primary cause (mantle transmission and/or defocusing). The seismogram from location R_1 shows that early Lg arrivals have high amplitude but later arrivals are considerably weaker. The effects of crustal thinning are not evident at this location and the weaker signal is explained entirely by propagation across the transition to thicker crust. The method of attenuation is defocusing. The slower ray paths reaching location R_1 are reflected in areas of Moho curvature and as a result, average geometric spreading is increased by a factor of 2. Since Moho curvature is found to cause attenuation in this and other program runs, it is useful to consider an alternative transition model; a planar dipping Moho. The planar surface will not cause the increase in geometric spreading noted above, but will result in attenuation through other means. Specifically, much of the defocused energy that reaches the receiver through curved transitions is reflected by planar transitions in directions that do not reach the receiver. This is easily visualized by considering rays tubes and the area between rays, which is the wavefront. Defocusing leads to larger wavefronts which have a better chance of reaching the receiver than do the smaller wavefronts.

reflected by planar surfaces. The present study has compared the methods and found comparable levels of attenuation, although the seismograms are somewhat different in appearance.

A very slight increase in attenuation is evident at receiver location R_2 , primarily because all rays reaching this point are defocused to some extent. Attenuation at location R_3 is quite a bit stronger than at R_1 and R_2 . Here the propagation path crosses the transition to thinner crust, which diverts much of the energy that would otherwise reach the receiver. Diversion occurs in three ways. First, rays travelling at post-critical angles relative to the horizontal Moho become pre-critical at the upward dipping transition, and energy is lost to mantle transmission. Secondly, a large portion of the remaining reflected energy travels at pre-critical angles, leading to mantle transmission beyond the transition. The third method of diversion is back-reflected rays.

Propagation Parallel to a Mountain Range

Figure 2 illustrates the results of tests of L_g propagation parallel to the strike of a mountain range for a vertical point force. Sources and receivers are assumed to lie within a mountain range having a deep crustal root. Seismogram trace 1 shown again for reference propagation in a crust having planar free surface and Moho. Traces 2-4 correspond to receiver locations R_1 , R_2 and R_3 . Transition zones trending parallel to the propagation path form a secondary waveguide and the modeling predicts that rays will be trapped within. These raypaths are weak, however, as Moho curvature causes significant attenuation by geometric spreading. The seismogram at location R_1 , which is not subject to transitions perpendicular to propagation, shows energy roughly equal to undisturbed L_g . Although a large number of raypaths with lateral reflections were traced, the increased geometric spreading leads to weak arrivals. The traces at locations R_2 and R_3 are seen to be strongly attenuated by the crustal thinning transition.

Rays trapped by the lateral waveguide undergo conversion between SV and SH, but conversions of this type are not noticeable in the synthetic seismograms. It is possible that because these rays tend to be weak, the conversions are not noticeable. Another possibility is that SH to SV conversion is generally canceled by SV to SH conversion under the particular conditions of this model. In the real crust, the primary method of SV to SH conversion is scattering by small scale heterogeneities, which can not be considered under the constraints of ray theory.

Propagation Oblique to a Mountain Range

Figure 3 illustrates the attenuation of L_g for paths oblique to the strike of a mountain range for a vertical point force. Sources and receivers are located such that propagation paths are at 90, 70, 45 and 20 degrees relative to the waveguide perturbations. Receiver distance is 2000 km in all cases. Strong attenuation is evident over each propagation path, but the individual waveforms vary considerably. For paths terminating at receivers R_1 and R_2 , rays encounter steep thickness transitions and many rays are entirely transmitted to the mantle. Along the more oblique paths leading to R_3 and R_4 , the Moho dips less steeply and as a result, the number of two-point ray paths increases. It appears that L_g propagates slightly more efficiently at 45 degrees than at the other angles tested, but the difference is insignificant compared to the level of attenuation.

Width of Crustal Transition

In crustal models shown in figure 1a, 4a and 4b, the width of the transition region between thick and thin crust is varied. The source-receiver paths are 2000 km in length and perpendicular to the strike of the transition regions. Synthetic traces 2 and 3 in Figure 4c, which compare a 200 km width of thickened crust with a 500 km width, both show weak Lg. The similarity between traces suggests that the width of a mountainous region has very little effect on overall attenuation. Trace 4 shows Lg after propagation through transition regions 200 km wide (compared to 100 km wide in trace 2) and the difference is readily apparent. The widened transition width results in Lg amplitude analogous to that in the undisturbed waveguide, which implies that the width of crustal transition regions and the corresponding change in overall Moho dip angle impose the primary control over Lg attenuation.

Propagation Across the Tibet Plateau

The map shown in Figure 5a gives source and receiver locations used in the Lg analysis of Razaikin et al. (1977). Shading corresponds to regions of high mountains. Central Asia was chosen to test the methods of the present study because Lg is known to be highly attenuated here and good specific examples are given in published seismograms. A study of focal mechanisms in the Tibetan Plateau (Molnar and Chen, 1983) found these earthquakes to occur at depths of 5 to 10 km with combined strike-slip and normal faulting and T axis primarily east-west. No earthquakes were located below 10 to 15 km, suggesting the crust is essentially aseismic below these depths. The fault solutions indicate the Tibetan Plateau is undergoing east-west extension, much like the Basin and Range province of the Western United States.

Crustal thickness has been hand digitized and the results, in the form of a Moho depth plot, are shown in Figure 5b. Samples are taken at a .5 degree (50 km) sampling of latitude and longitude. (Topography and Moho depth at 10 km sampling are now available in unclassified databases established by Fielding et al., 1992.) The method of determining crustal thickness is a combination of published survey results and inference. Choudary, 1975 estimates crustal thickness of 70-72 km in the Central Himalayas from Bouger gravity anomalies. Bird and Toksoz, 1975 study the velocity of 20-80 second Rayleigh waves and conclude that the crust is 75 km thick within the Tibetan Plateau. Published data on crustal thickness within the Tarim Basin and Tien Shan Mountains were not found, so thickness has been estimated from average elevation. Elevation varies from 500 to 1000 meters within the Tarim Basin and crustal thickness is estimated at 35 km. Average Tien Shan elevation is on the order of 3000 meters, leading to a thickness estimate of 50 km. Estimation of crustal thickness combined with the large digital sampling intervals lead to a very rough model of the crust, but the transitions, which seem to most strongly effect Lg propagation, are represented as closely as the model will allow.

Figure 5a shows propagation paths from the two earthquakes chosen for modeling by the ray method. Double couple radiation patterns have been included. Both paths are subject to crustal thinning at the Tarim Basin then crustal thickening at the Tien Shan mountains before the waves are recorded at Soviet station Talgar (TLG). Since the paths are similar, transition steepness will be approximately the same. The main difference between paths is that the the more westerly path

from the earthquake near 87°E longitude travels about half as far within the Tibetan Plateau as the path from the earthquake near 93° longitude. Figures 6a,b compare the observed and synthetic seismogram for the earthquake ($m_b=5.1$) having the more westerly path. Lg appears to be strongly transmitted, having a high amplitude relative to Pn. The synthetic agrees well with details of the observed Lg coda. Figures 7a,b compare seismograms recorded from earthquake ($m_b=6.1$) having the more easterly path. Lg appears to be very weak in these recordings, having a low amplitude relative to Pn. The synthetic seismogram has high amplitude pulses not seen in the observed seismogram.

Certain additions to the crustal model could significantly improve the match between the synthetics and the recordings. First, inclusion of the low Q believed to exist in the deep crust of the Tibetan Plateau (Bird and Toksoz, 1975) would improve the agreement between observed and predicted Lg transmission. Each ray incident at the Moho beneath the Tibetan Plateau would be subject to high intrinsic attenuation, establishing a direct relationship between travel distance within the plateau and attenuation suggested by the observations. Scattering attenuation by the 3-D heterogeneities associated with the uplifted region would tend to reinforce this relationship. Details of the shallow structure of the Tarim Basin have been omitted from the crustal model. The weak path, for which poor agreement exists between observed and predicted Lg transmission, crosses the Tarim Basin. Baumgardt (1991) found that sedimentary basin structure is at least as important, if not more important, than Moho topography in controlling Lg propagation. Low seismic velocity within the sediments can form a waveguide trapping a significant portion of the rays that would otherwise contribute to Lg, the slopes of the basin on exiting side rays acting to defocus subsequent SmS rays (Figure 8). Rays reverberating within the sedimentary basin would also suffer high levels of scattering attenuation within the sediments. A third possibility for the discrepancy between the observed and predicted Lg waveforms in the weak path example is suggested by comparing the topographically inferred Moho with that determined by the Soviet Deep Seismic Sounding Project (DSS). In the region of the Tibet Plateau, the transition zone between normal and thickened crust is quite different in form in DSS sections than that which would be predicted by simple isostasy (Fielding, personal communication). One or more of these modifications of the crustal model may lead to synthetics that more closely match the attenuation levels seen in the recorded seismograms.

Scattering Within the Crustal Waveguide

The modeling described in the previous subsections does a remarkably good job in predicting the blocking of Lg by major crustal transitions and is often successful in accounting for the most significant details of the Lg coda. It is clear, however, that observed Lg codas will be always contain greater complexity than synthetic codas generated in models having a homogeneous crust. We have conducted several experiments to include the effects of fine scale three-dimensional heterogeneities within a crustal waveguide of variable thickness. To achieve this goal, we added dynamically traced rays to point scatterers within a crustal waveguide of variable thickness (Figure 9). A standard Born approximation (e.g., Wu and Aki, 1985) is used to calculate the radiation pattern of the point scatterers. The results shown in Figure 9 were calculated for a single point heterogeneity having positive 5 per cent contrasts in P velocity, S velocity, and density from the background medium.

It is clear that the existence of even a single point heterogeneity quickly acts to fill up the coda between multiply reflected S waves.

The standard Born approximation used in this demonstration does not conserve energy and does a poor job in recreating scattered codas predicted by finite difference solutions of the elastic equation of motion in heterogeneous media (Coates and Charrette, 1992). Improved agreement with finite difference simulations can be obtained by using the generalized Born approximation (Coates and Chapman, 1991). The generalized Born approximation, in which scattering occurs by a process of frequency dependent reflection by regions of high gradient, is applicable to models in which velocities and density are parameterized by continuous functions of space. Such a parameterization also greatly simplifies the description of the rays contributing regional seismograms.

Importance of Scattering in Different Depth Regions of the Crust

Lg rays have been dynamically traced in models of the crust in which the Moho has been represented by a high gradient transition (Figure 10). The SmS rays contributing to the Lg coda are turning rays in the high gradient region. Geometric spreading factors have been tracked along each ray, demonstrating that the spreading factors of individual rays vanish at the turning points within the Moho transition. It is well known that such a high gradient zone will form a caustic surface within the high gradient zone, to which multiple turning rays will be tangent. A reversed travel time branch and triplication will also be observed for rays traced at a sequence of increasing take-off angles. Scattering of Lg rays near the caustic surface, where amplitudes will be high due to the vanishing of the geometric spreading factor, will be greatly enhanced. This situation is very analogous to the enhanced amplitude of scattered PKIKP precursors due to heterogeneity at the core mantle boundary (e.g., Bataille and Flotte, 1988). For PKIKP precursors, the presence of a caustic surface in the outer core is sufficient to make even a very slight heterogeneity near the core-mantle boundary account for the observed amplitudes of the scattered waves. Likewise, a caustic surface within a Moho transition zone will be capable of amplifying the effects of very slight heterogeneity within the Moho transition.

In predicting regions in which enhanced scattering may occur it is also useful to consider the intersections of SmS rays traced from the receiver with SmS rays that originate at the source. In two-dimensional scattering, the existence of a heterogeneity at such crossing points will make it possible for SmS to SmS scattering to occur, filling up the coda between the individual SmS arrivals making up the Lg coda. The greatest density of such crossing points occurs near the Moho transition and near the free surface. An important source of the late Lg coda will be three-dimensional SmS to SmS scattering occurring out of the vertical plane containing the source and receiver.

CONCLUSIONS AND RECOMMENDATIONS

Modeling Results

(1) Moho Topography and Sedimentary Basins are the two most important elements structures responsible for Lg blockage.

(2) Slopes of major crustal discontinuities and transitions (Moho and basin-sediment interface) are the principal features controlling the propagation efficiency of Lg.

(3) There is only a weak dependence on the azimuth of the propagation path with respect to the strike of blocking features.

(4) Distributed heterogeneities and small scale topography of crustal discontinuities in the crust can act to fill up and lengthen the Lg coda. Heterogeneities within the crust primarily along the source-receiver azimuth fill up the early coda between individual S waves trapped in the crustal waveguide. Off azimuth heterogeneities within the crust are a significant component of the late Lg coda following the last arriving Moho reflected S wave.

Lessons from Ray Based Approaches to Regional Seismogram Synthesis

(1) Utility of a Continuous Model Parameterization: The complexity of ray code descriptions in models described by first order discontinuities argues for models parameterized by functions continuous in space.

(2) Treatment of Reflections and Conversions in Regions of Strong Gradient: A generalized Born approximation can be used to calculate the frequency dependent scattering by regions having strong gradient, including the Moho transition zone resulting from the parameterization described above.

(3) The Most Important Regions of Scattering for the Lg Phase and Why:

(a) Moho transition because a caustic surface is included in this region for many of the S waves composing the Lg phase. In addition there is a high density of S ray intersections in this region permitting scattering from one type of multiply reflected S wave composing the Lg phase to another type.

(b) The free surface region because there is a high density of S ray intersections in this region permitting scattering from a source ray consisting of multiple Moho reflected S waves to a receiver ray consisting of multiply reflected S waves. In addition, this region should be important based on array data suggesting a higher magnitude of velocity and density fluctuations in the upper 2 km of the crust.

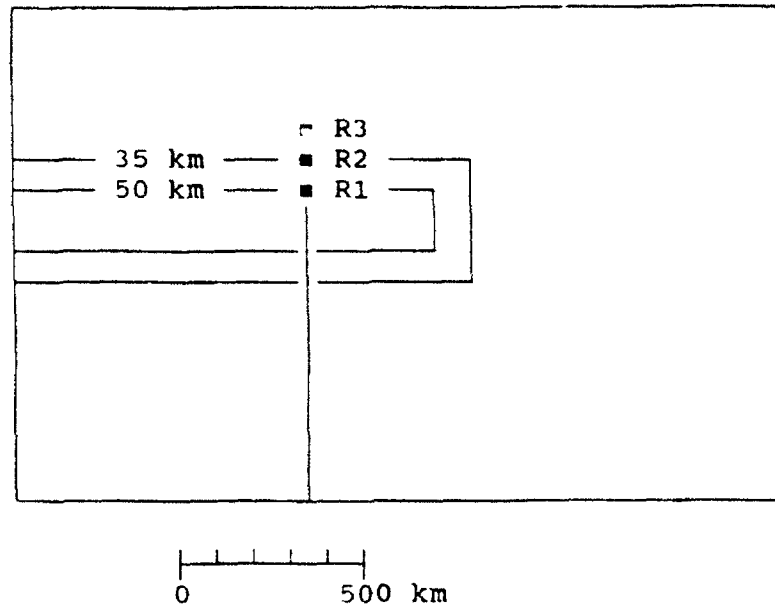
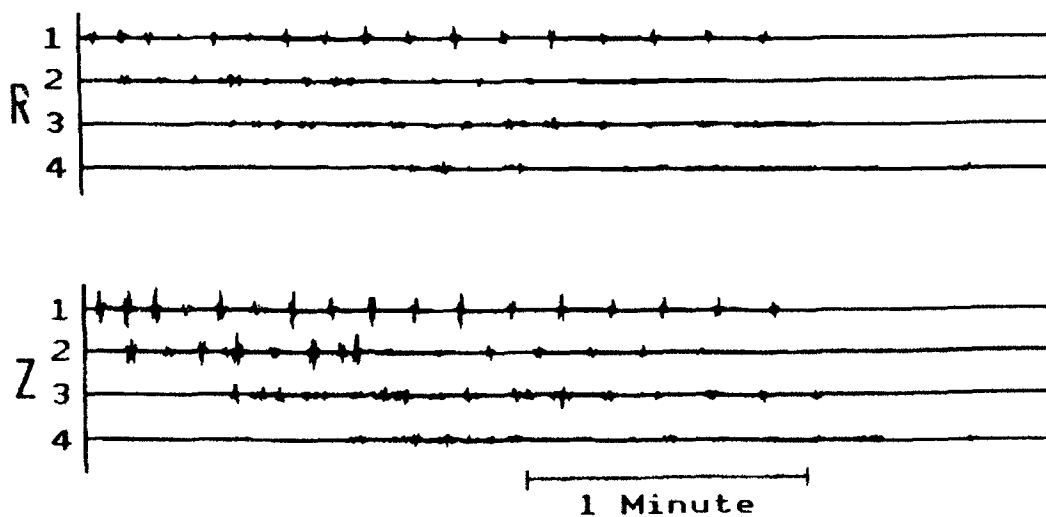


Figure 1 (a) Above: propagation paths normal to strike of mountain range. This map view shows the crustal thickness contours of a narrow hypothetical mountain belt, along with the Lg propagation path and receiver locations. R_1 through R_3 offsets are 2200, 2300, and 2400 km respectively. an unperturbed waveguide. (b) Below: ray synthetic seismograms for paths to receivers R_1 through R_3 . Trace 1 is Lg modeled at the R_1 offset in an unperturbed waveguide. Transverse ground motion is not shown because SV to SH conversion does not occur when the propagation path is perpendicular to waveguide variations.



Trace 1 = Non-attenuated Lg
 Trace 2 = Receiver R_1
 Trace 3 = Receiver R_2
 Trace 4 = Receiver R_3

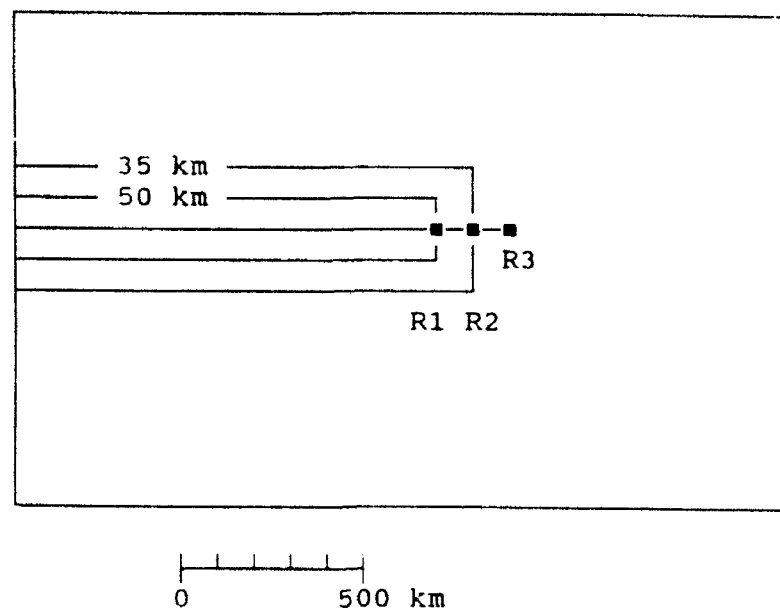
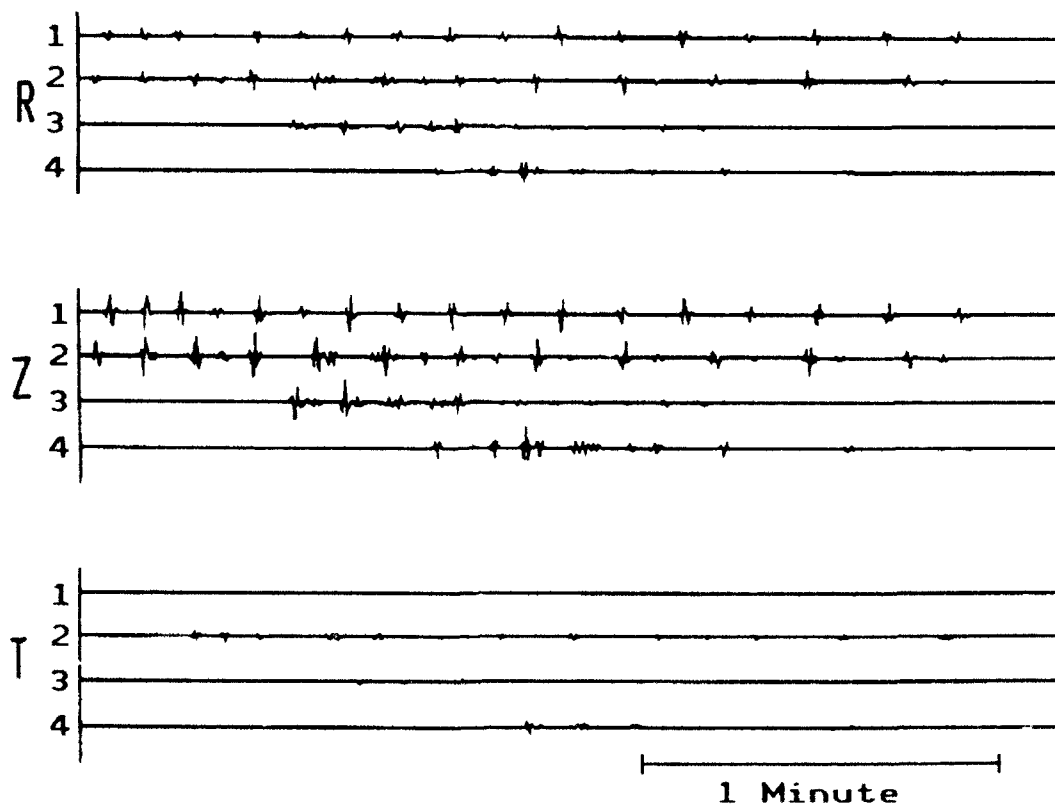


Figure 2 (a) Above: propagation paths parallel to the strike of the mountain range. Offsets are 2200, 2300, and 2400 km. to receivers within the mountain range. (b) Below: ray synthetic seismograms. An increased number of ray paths reach receiver R_1 relative to receivers R_2 and R_3 resulting from lateral reflections within the mountain belt. Coda duration is sharply limited at the R_2 and R_3 . Very weak motion can be seen on the transverse traces.



Trace 1 = Non-attenuated Lg
 Trace 2 = Receiver R_1
 Trace 3 = Receiver R_2
 Trace 4 = Receiver R_3

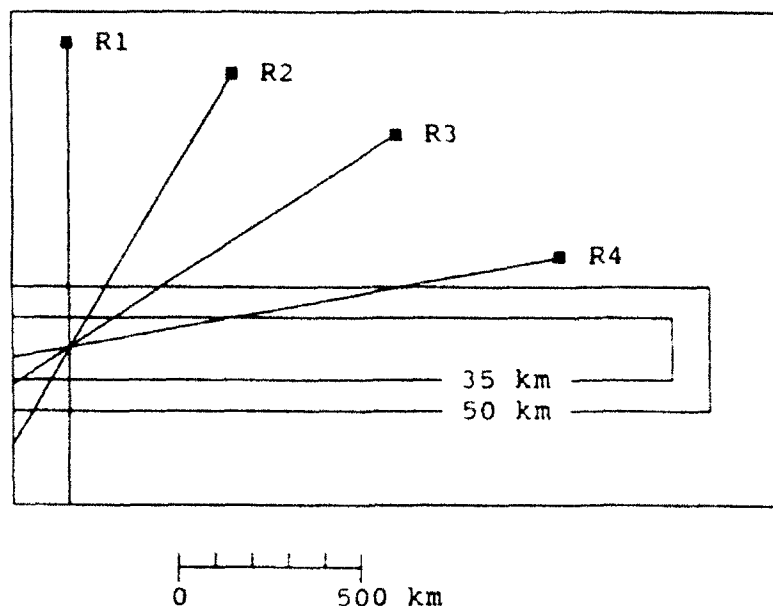
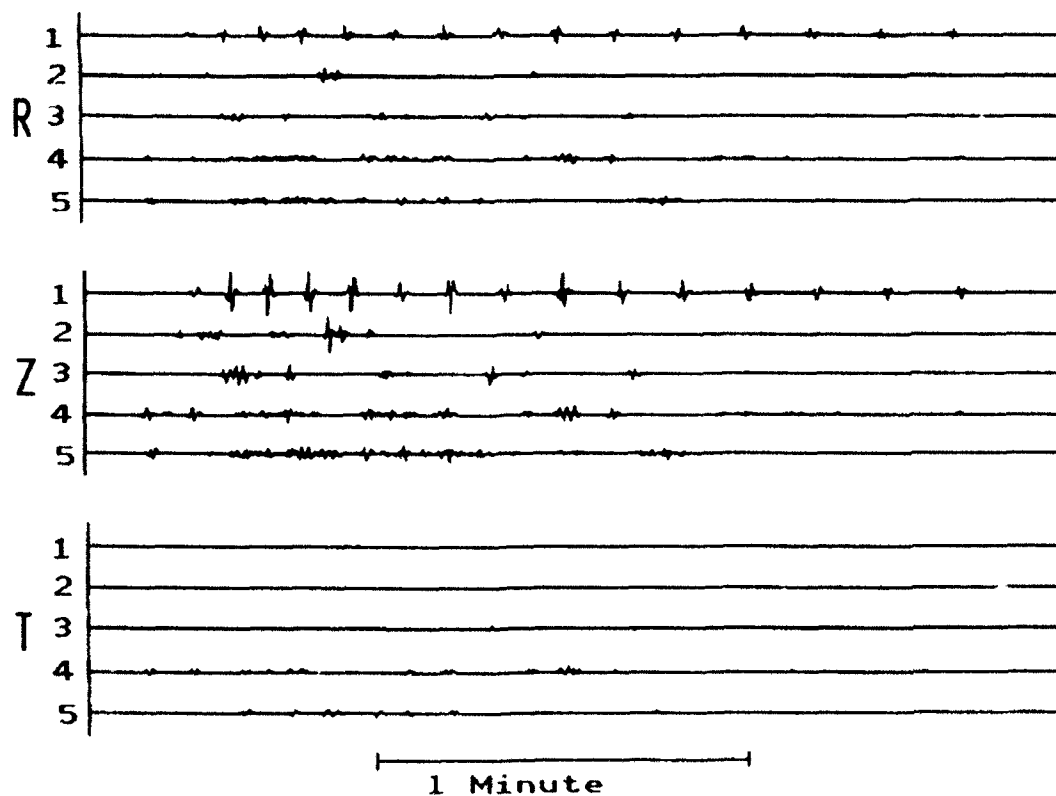


Figure 3 Lg propagation at paths making oblique angles to the strike of the mountain range. Above: (a) path to R_1 is at 90° , path to R_2 is at 70° , path to R_3 is at 45° , and path to R_4 is at 20° . Receiver offset is 2000 km over all paths. Below: (b) ray synthetic seismograms. Although waveforms 2-5 vary considerably, all have been considerably attenuated relative to the reference trace in an unperturbed waveguide and total energy is roughly the same for each of these paths.



Trace 1 = Non-attenuated Lg
 Trace 2 = Receiver R_1 (90 degrees)
 Trace 3 = Receiver R_2 (70 degrees)
 Trace 4 = Receiver R_3 (45 degrees)
 Trace 5 = Receiver R_4 (20 degrees)

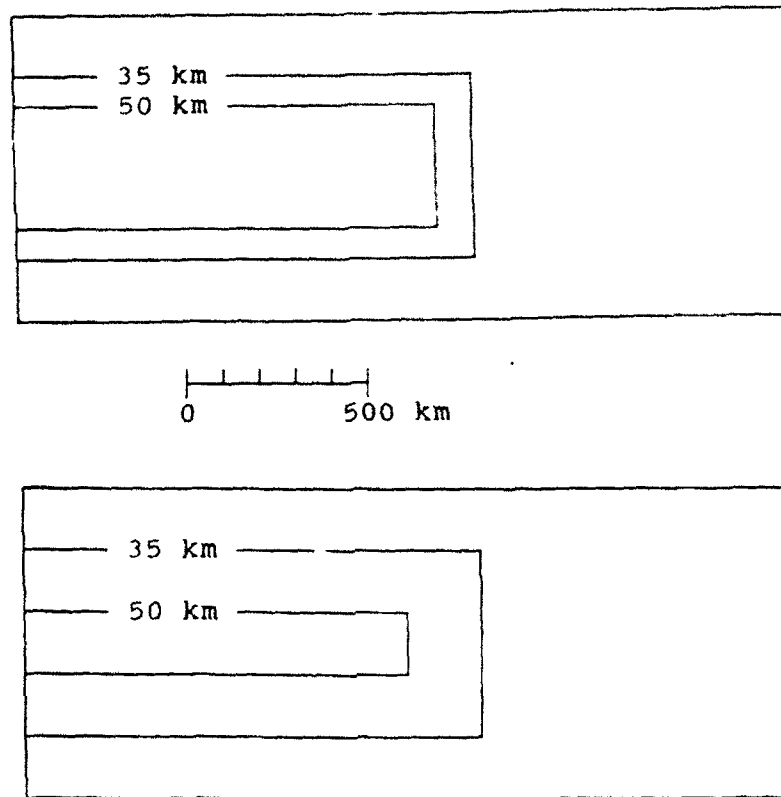
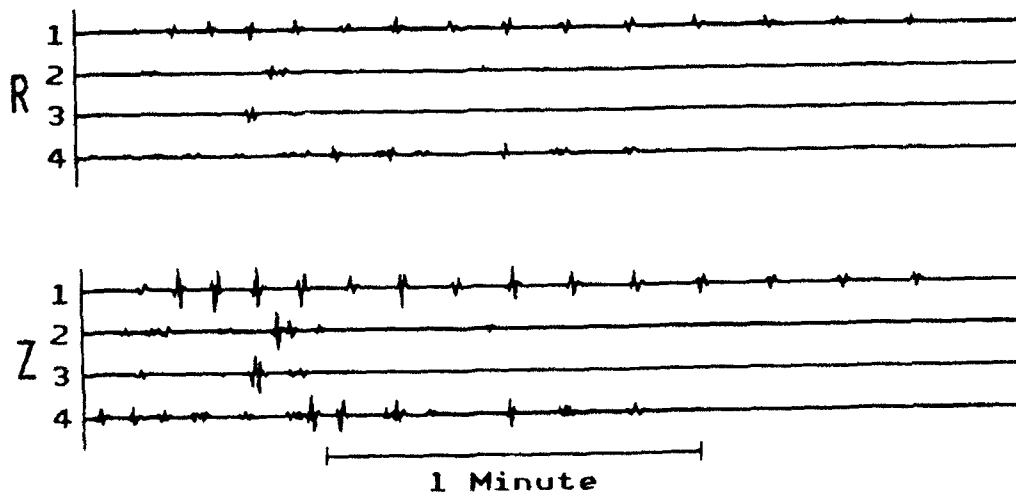


Figure 4 Effect of the width of crustal thickening and thinning. The crust increases and decreases in thickness over transition regions 100 km (above) and 200 km (middle). Ray synthetic Lg wavetrains are shown below for an offset of 2000 km and propagation perpendicular to the strike of the mountain range. Weak Lg in traces 2 and 3 compared to strong Lg in trace 4 indicates that the width of the transition region affects Lg efficiency more than the overall width of the mountain root.



- Trace 1 = Non-attenuated Lg
- Trace 2 = Receiver R₁ Crust Model 1a
- Trace 3 = Receiver R₂ Crust Model 4a
- Trace 4 = Receiver R₃ Crust Model 4b

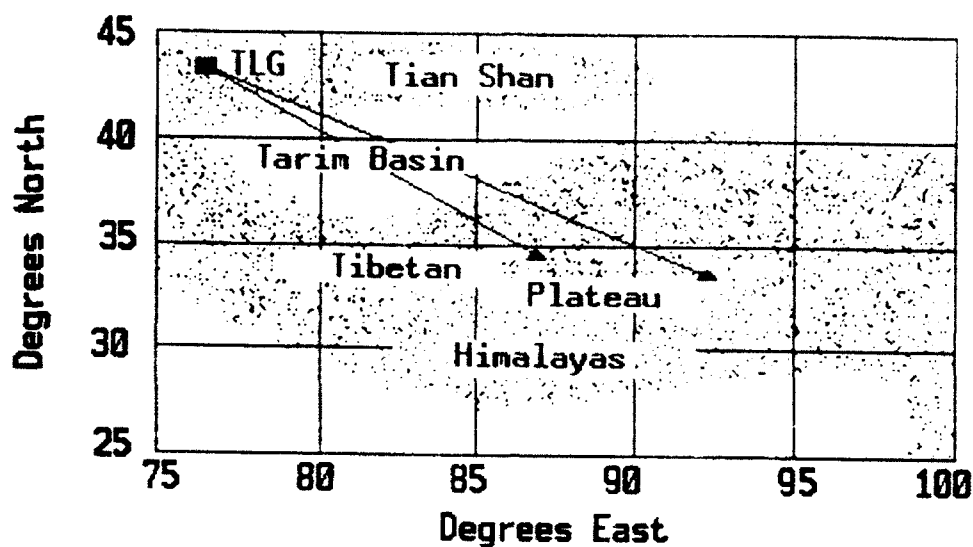
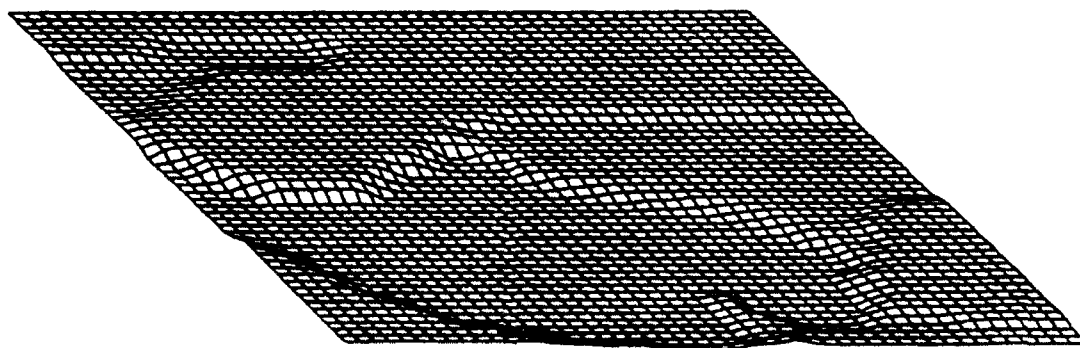


Figure 5 Above: (a) map of Central Asia showing the propagation paths of two earthquakes modeled by ray methods. Shading highlights high mountainous regions of thickened crust. The left path gives a detectable Lg signal and is referred to as the strong path. Lg from the right earthquake is very weak. Below: (b) Central Asian Moho depth plot obtained by digitization of crustal thickness values. Not to scale.



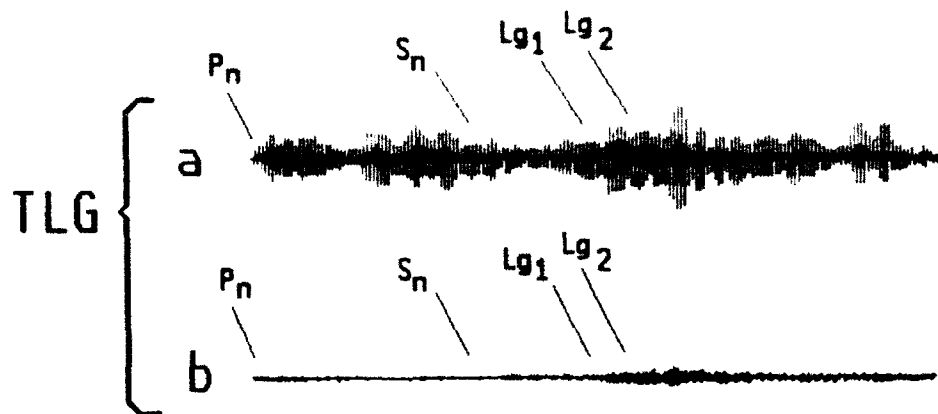
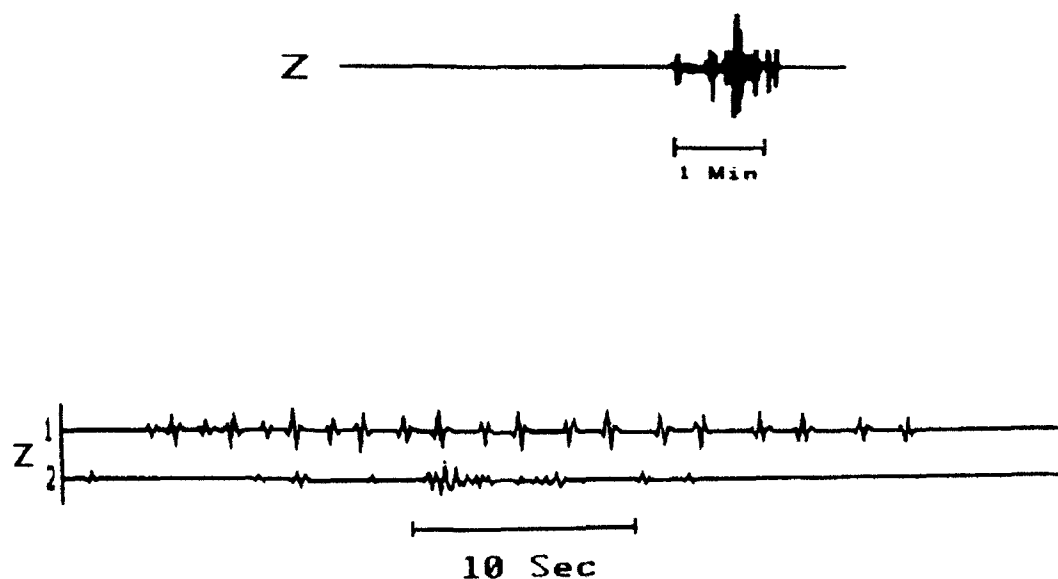


Figure 6 Above: (a) Central Asia strong path seismograms. The seismograms recorded from the left earthquake of figure 5a show clear Lg energy in both the top trace (instrument response peaked between 0.5 to 1 Hz.) and bottom trace (instrument response peaked between 0.2 to 0.5 Hz.). Middle: (b) scaled strong path synthetic. The synthetic seismogram is scaled to the dimensions of the actual seismogram and shows good recreation of Lg. Below (c): detailed strong path synthetic. These synthetic seismograms are not scaled to the recordings and allow determination of the level of attenuation. Ray modeling through a homogeneous crust predicts significant attenuation over this path.



Trace 1 = Non-attenuated Lg
Trace 2 = Strong path synthetic

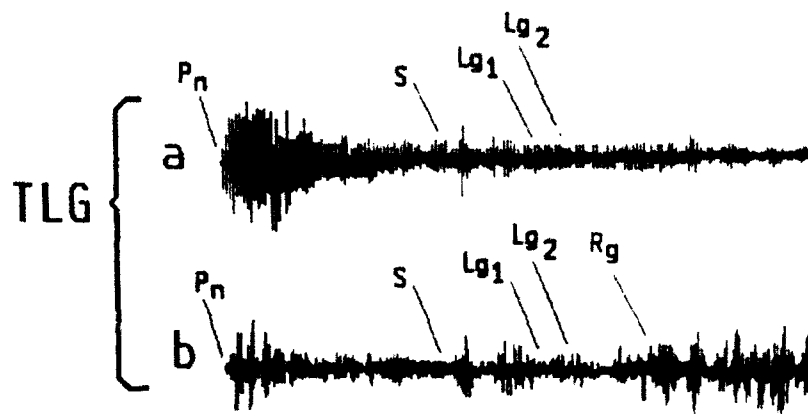
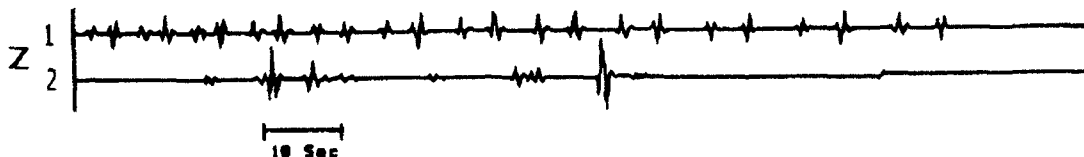
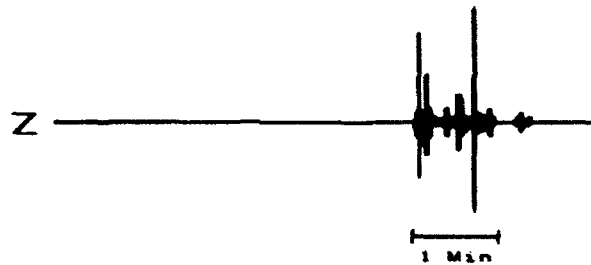


Figure 7 Above: (a) Central Asia weak path seismograms. The seismograms recorded from the right earthquake of figure 5a show very weak Lg, as can be seen by comparing Lg amplitude to Pn. Middle: (b) scaled weak path synthetic. The synthetic seismogram of the weak path predicts energetic pulses that are not present in the actual recordings. Below: (c) detailed weak path synthetic. Lg is clearly attenuated over this path but, as seen in figure 9b, the predicted level of attenuation is insufficient to explain the observations.



Trace 1 = Non-attenuated Lg
Trace 2 = Weak path synthetic

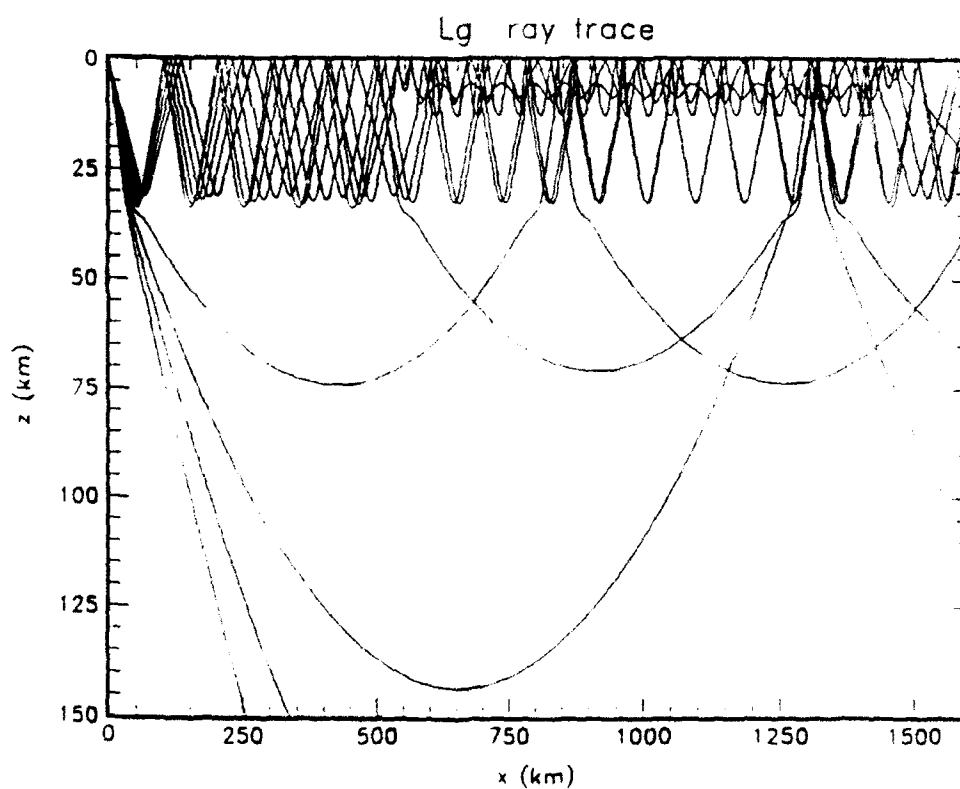
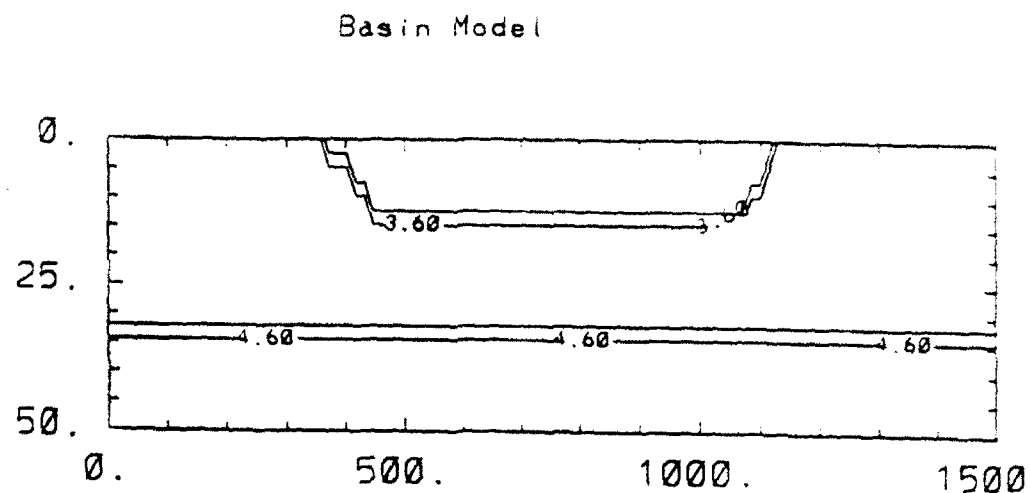


Figure 8. Top: Iso-S velocity contours defining a deep sedimentary basin (Z and X-coordinates are in kilometers.) Bottom: ray trace of S waves trapped in the crustal waveguide (Lg). Note that the effect of the basin will be to attenuate Lg at stations 1400 km and greater range.

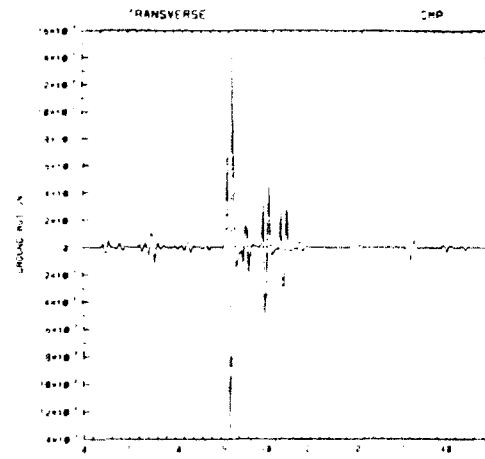
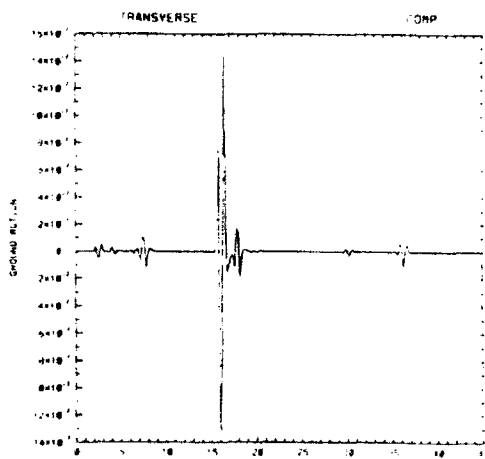
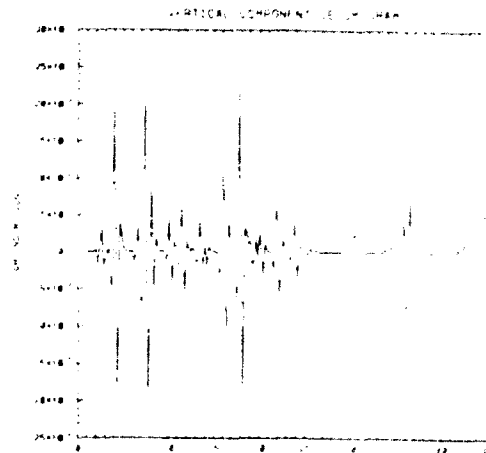
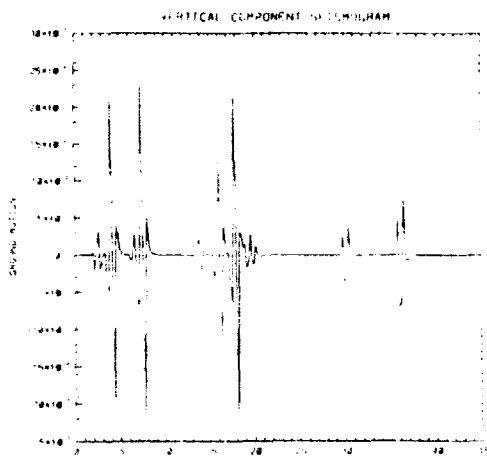
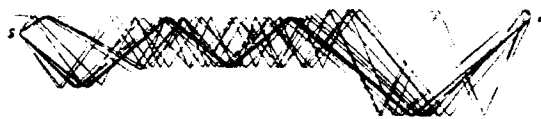


Figure 9. Effect of scattering within a crustal waveguide of variable thickness. Left column: no scattering within the crustal waveguide. Right column: scattering by a single scatterer within the crustal waveguide. (In the synthetics shown in the right column, all of the ray paths shown at top left are included plus the scattering paths shown at top right.)

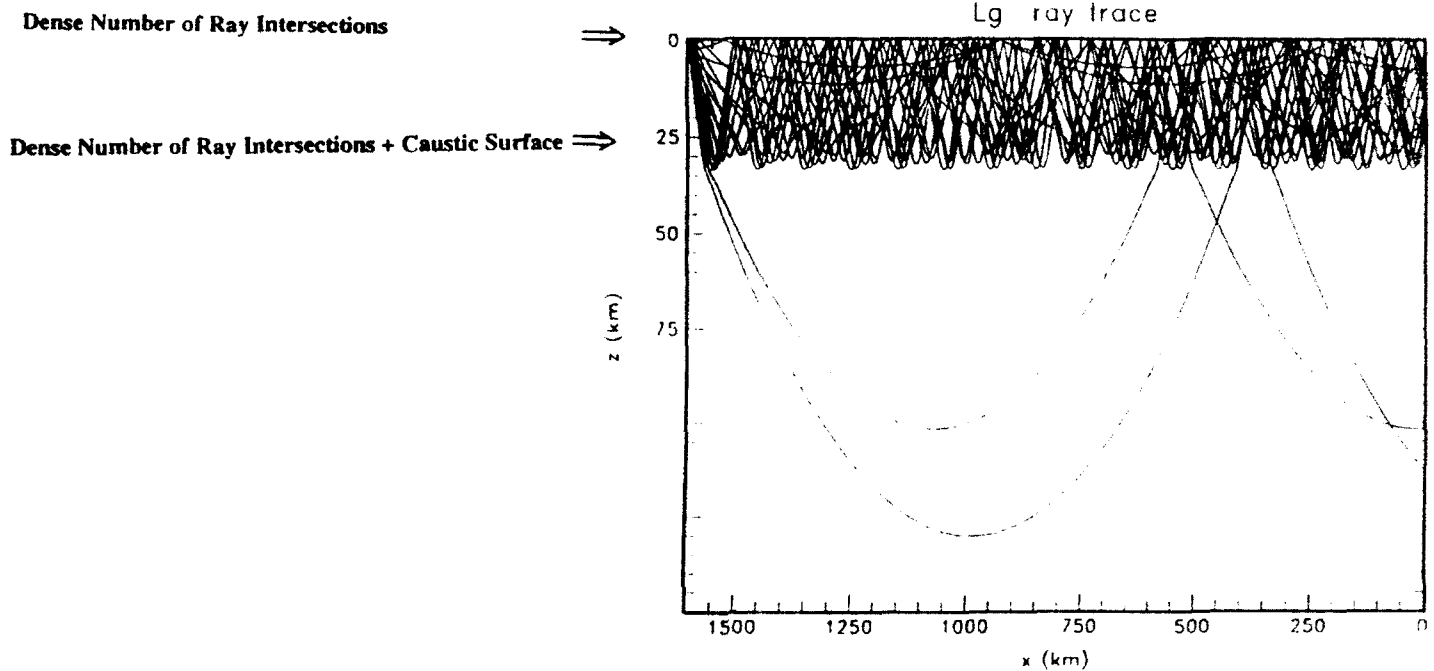


Figure 10. Intersections of rays traced from the receiver with rays traced from the source are densest near the surface and near the SmS turning points. Scatterers at these locations will contribute to the complexity of Lg coda. Scattering near the Moho transition will be particularly important because the presence of a caustic in this region will greatly amplify the effects of small perturbations in elastic moduli and density.

REFERENCES

- Bataille, K., and S.M. Flatte, Inhomogeneities near the core-mantle boundary inferred from short-period scattered PKP waves recorded at the Global Digital Seismogram Network, *J. Geophys. Res.*, **93**, 15057-15064, 1988.
- Bird, P. and M.N. Toksoz, Structure and evolution of the Tibetan Plateau, *EOS, Trans. Am. Geophys. Union* **56**, 397, 1975.
- Baumgardt, D.R., High frequency array studies of long range Lg propagation and the causes of Lg blockage and attenuation in the Eurasian continental craton, Final Report, PL-TR-91-2059(11), Phillips Laboratory, Hanscom AFB, MA, 1991, ADA236984.
- Červený, V., The application of ray tracing to the propagation of shear waves in complex media, in *Seismic Exploration*, pp. 1-124, Treitel and Helbig, Vol. on Seismic Shear Waves, G. Doherty, ed., Geophysical Press, 1985.
- Choudary, S.K., Gravity and crustal thickness in the Indo-Gangetic Plains and Himalayan region, India, *Geophys. J. R. Astr. Soc.* **40**, 441-452, 1975.
- Coates, R.T., and C.H. Chapman, Generalized Born scattering of elastic waves in 3-D media, *Geophys. J. Int.*, **107**, 321-363, 1991.
- Coates, R.T., and Charrette, E.E., A comparison of single scattering and finite difference synthetic seismograms in realizations of 2-D elastic random media, *Geophys. J. Int.*, in press, 1992.
- Cormier, V.F., and M. Kalmbach, Lg Propagation in Mountainous Regions In: Crustal and Upper Mantle Gradients in the Vicinity of the East Kazakh Test Site, Scientific Report No. 1, PL-TR-91-2215, Phillips Laboratory, Hanscom AFB, MA, 1991, ADA246889.
- Fielding, E., B.L. Isacks, and M. Barazangi, A Network Accessible Geological and Geophysical Database for Eurasia, Proceedings of the 14th Annual PL/DARPA Seismic Research Symposium, 16-18 September, 1992, PL-TR-92-2210, Phillips Laboratory, Hanscom AFB, MA, 1992, ADA256711.
- Kennett, B.L.N., Lg waves and structural boundaries, *Bull. Seism. Soc. Am.* **76**, 1133-1144, 1986.
- Molnar, P. and W. Chen, Focal depths and fault plane solutions of earthquakes under the Tibetan Plateau, *J. Geophys. Res.* **88**, 1180-1196, 1983.
- Press, F. and R. Siever, *Earth*, W.H. Freeman and Co., 1982.
- Ruzaikin, A.I., I.L. Nersesov, V.I. Khalturin and P. Molnar, Propagation of Lg and lateral varia-

tions in crustal structure in Asia, *J. Geophys. Res.* 82, 307-316, 1977.

Wu, R.-S., and K. Aki, Scattering characteristics of elastic waves by elastic heterogeneity, *Geophysics*, 50, 582-595, 1985.

Prof. Thomas Ahrens
Seismological Lab, 252-21
Division of Geological & Planetary Sciences
California Institute of Technology
Pasadena, CA 91125

Prof. Keiiti Aki
Center for Earth Sciences
University of Southern California
University Park
Los Angeles, CA 90089-0741

Prof. Shelton Alexander
Geosciences Department
403 Deike Building
The Pennsylvania State University
University Park, PA 16802

Dr. Ralph Alewine, III
DARPA/NMRO
3701 North Fairfax Drive
Arlington, VA 22203-1714

Prof. Charles B. Archambeau
CIRES
University of Colorado
Boulder, CO 80309

Dr. Thomas C. Bache, Jr.
Science Applications Int'l Corp.
10260 Campus Point Drive
San Diego, CA 92121 (2 copies)

Prof. Muawia Barazangi
Institute for the Study of the Continent
Cornell University
Ithaca, NY 14853

Dr. Jeff Barker
Department of Geological Sciences
State University of New York
at Binghamton
Vestal, NY 13901

Dr. Douglas R. Baumgardt
ENSCO, Inc
5400 Port Royal Road
Springfield, VA 22151-2388

Dr. Susan Beck
Department of Geosciences
Building #77
University of Arizona
Tucson, AZ 85721

Dr. T.J. Bennett
S-CUBED
A Division of Maxwell Laboratories
11800 Sunrise Valley Drive, Suite 1212
Reston, VA 22091

Dr. Robert Blandford
AFTAC/IT, Center for Seismic Studies
1300 North 17th Street
Suite 1450
Arlington, VA 22209-2308

Dr. Stephen Bratt
Center for Seismic Studies
1300 North 17th Street
Suite 1450
Arlington, VA 22209-2308

Dr. Lawrence Burdick
Woodward-Clyde Consultants
566 El Dorado Street
Pasadena, CA 91109-3245

Dr. Robert Burrridge
Schlumberger-Doll Research Center
Old Quarry Road
Ridgefield, CT 06877

Dr. Jerry Carter
Center for Seismic Studies
1300 North 17th Street
Suite 1450
Arlington, VA 22209-2308

Dr. Eric Chael
Division 92-41
Sandia Laboratory
Albuquerque, NM 87185

Dr. Martin Chapman
Department of Geological Sciences
Virginia Polytechnical Institute
21044 Derring Hall
Blacksburg, VA 24061

Prof. Vernon F. Cormier
Department of Geology & Geophysics
U-45, Room 207
University of Connecticut
Storrs, CT 06268

Prof. Steven Day
Department of Geological Sciences
San Diego State University
San Diego, CA 92182

Marvin Denny
U.S. Department of Energy
Office of Arms Control
Washington, DC 20585

Dr. Cliff Frolich
Institute of Geophysics
8701 North Mopac
Austin, TX 78759

Dr. Zoltan Der
ENSCO, Inc.
5400 Port Royal Road
Springfield, VA 22151-2388

Dr. Holly Given
IGPP, A-025
Scripps Institute of Oceanography
University of California, San Diego
La Jolla, CA 92093

Prof. Adam Dziewonski
Hoffman Laboratory, Harvard University
Dept. of Earth Atmos. & Planetary Sciences
20 Oxford Street
Cambridge, MA 02138

Dr. Jeffrey W. Given
SAIC
10260 Campus Point Drive
San Diego, CA 92121

Prof. John Ebel
Department of Geology & Geophysics
Boston College
Chestnut Hill, MA 02167

Dr. Dale Glover
Defense Intelligence Agency
ATTN: ODT-1B
Washington, DC 20301

Eric Fielding
SNEE Hall
INSTOC
Cornell University
Ithaca, NY 14853

Dr. Indra Gupta
Teledyne Geotech
314 Montgomery Street
Alexandria, VA 22314

Dr. Mark D. Fisk
Mission Research Corporation
735 State Street
P.O. Drawer 719
Santa Barbara, CA 93102

Dan N. Hagedorn
Pacific Northwest Laboratories
Battelle Boulevard
Richland, WA 99352

Prof Stanley Flatte
Applied Sciences Building
University of California, Santa Cruz
Santa Cruz, CA 95064

Dr. James Hannon
Lawrence Livermore National Laboratory
P.O. Box 808
L-205
Livermore, CA 94550

Dr. John Foley
NER-Geo Sciences
1100 Crown Colony Drive
Quincy, MA 02169

Dr. Roger Hansen
HQ AFTAC/TTR
Patrick AFB, FL 32925-6001

Prof. Donald Forsyth
Department of Geological Sciences
Brown University
Providence, RI 02912

Prof. David G. Harkrider
Seismological Laboratory
Division of Geological & Planetary Sciences
California Institute of Technology
Pasadena, CA 91125

Dr. Art Frankel
U.S. Geological Survey
922 National Center
Reston, VA 22092

Prof. Danny Harvey
CIRES
University of Colorado
Boulder, CO 80309

Prof. Donald V. Helmberger
Seismological Laboratory
Division of Geological & Planetary Sciences
California Institute of Technology
Pasadena, CA 91125

Prof. Eugene Herrin
Institute for the Study of Earth and Man
Geophysical Laboratory
Southern Methodist University
Dallas, TX 75275

Prof. Robert B. Herrmann
Department of Earth & Atmospheric Sciences
St. Louis University
St. Louis, MO 63156

Prof. Lane R. Johnson
Seismographic Station
University of California
Berkeley, CA 94720

Prof. Thomas H. Jordan
Department of Earth, Atmospheric &
Planetary Sciences
Massachusetts Institute of Technology
Cambridge, MA 02139

Prof. Alan Kafka
Department of Geology & Geophysics
Boston College
Chestnut Hill, MA 02167

Robert C. Kemerait
ENSCO, Inc.
445 Pineda Court
Melbourne, FL 32940

Dr. Karl Koch
Institute for the Study of Earth and Man
Geophysical Laboratory
Southern Methodist University
Dallas, Tx 75275

Dr. Max Koontz
U.S. Dept. of Energy/DP 5
Forrestal Building
1000 Independence Avenue
Washington, DC 20585

Dr. Richard LaCoss
MIT Lincoln Laboratory, M-200B
P.O. Box 73
Lexington, MA 02173-0073

Dr. Fred K. Lamb
University of Illinois at Urbana-Champaign
Department of Physics
1110 West Green Street
Urbana, IL 61801

Prof. Charles A. Langston
Geosciences Department
403 Deike Building
The Pennsylvania State University
University Park, PA 16802

Jim Lawson, Chief Geophysicist
Oklahoma Geological Survey
Oklahoma Geophysical Observatory
P.O. Box 8
Leonard, OK 74043-0008

Prof. Thorne Lay
Institute of Tectonics
Earth Science Board
University of California, Santa Cruz
Santa Cruz, CA 95064

Dr. William Leith
U.S. Geological Survey
Mail Stop 928
Reston, VA 22092

Mr. James F. Lewkowicz
Phillips Laboratory/GPEH
Hanscom AFB, MA 01731-5000(2 copies)

Mr. Alfred Lieberman
ACDA/VI-OA State Department Building
Room 5726
320-21st Street, NW
Washington, DC 20451

Prof. L. Timothy Long
School of Geophysical Sciences
Georgia Institute of Technology
Atlanta, GA 30332

Dr. Randolph Martin, III
New England Research, Inc.
76 Olcott Drive
White River Junction, VT 05001

Dr. Robert Masse
Denver Federal Building
Box 25046, Mail Stop 967
Denver, CO 80225

Dr. Gary McCartor
Department of Physics
Southern Methodist University
Dallas, TX 75275

Prof. Thomas V. McEvilly
Seismographic Station
University of California
Berkeley, CA 94720

Dr. Art McGarr
U.S. Geological Survey
Mail Stop 977
U.S. Geological Survey
Menlo Park, CA 94025

Dr. Keith L. McLaughlin
S-CUBED
A Division of Maxwell Laboratory
P.O. Box 1620
La Jolla, CA 92038-1620

Stephen Miller & Dr. Alexander Florence
SRI International
333 Ravenswood Avenue
Box AF 116
Menlo Park, CA 94025-3493

Prof. Bernard Minster
IGPP, A-025
Scripps Institute of Oceanography
University of California, San Diego
La Jolla, CA 92093

Prof. Brian J. Mitchell
Department of Earth & Atmospheric Sciences
St. Louis University
St. Louis, MO 63156

Mr. Jack Murphy
S-CUBED
A Division of Maxwell Laboratory
11800 Sunrise Valley Drive, Suite 1212
Reston, VA 22091 (2 Copies)

Dr. Keith K. Nakanishi
Lawrence Livermore National Laboratory
L-025
P.O. Box 808
Livermore, CA 94550

Dr. Carl Newton
Los Alamos National Laboratory
P.O. Box 1663
Mail Stop C335, Group ESS-3
Los Alamos, NM 87545

Dr. Bao Nguyen
HQ AFTAC/ITR
Patrick AFB, FL 32925-6001

Prof. John A. Orcutt
IGPP, A-025
Scripps Institute of Oceanography
University of California, San Diego
La Jolla, CA 92093

Prof. Jeffrey Park
Kline Geology Laboratory
P.O. Box 6666
New Haven, CT 06511-8130

Dr. Howard Paton
Lawrence Livermore National Laboratory
L 025
P.O. Box 808
Livermore, CA 94550

Dr. Frank Pilotte
HQ AFTAC/IT
Patrick AFB, FL 32925-6001

Dr. Jay J. Pulli
Radix Systems, Inc.
2 Taft Court, Suite 203
Rockville, MD 20850

Dr. Robert Reinke
ATTN: ECFTVTD
Field Command
Defense Nuclear Agency
Kirtland AFB, NM 87115

Prof. Paul G. Richards
Lamont-Doherty Geological Observatory
of Columbia University
Palisades, NY 10964

Mr. Wilmer Rivers
Teledyne Geotech
314 Montgomery Street
Alexandria, VA 22314

Dr. George Rothe
HQ AFTAC/ITR
Patrick AFB, FL 32925-6001

Dr. Alan S. Ryall, Jr.
DARPA/NMRC
3701 North Fairfax Drive
Arlington, VA 22209-1714

Dr. Richard Sailor
TASC, Inc.
55 Walkers Brook Drive
Reading, MA 01867

Prof. Charles G. Sammis
Center for Earth Sciences
University of Southern California
University Park
Los Angeles, CA 90089-0741

Prof. Christopher H. Scholz
Lamont-Doherty Geological Observatory
of Columbia University
Palisades, NY 10964

Dr. Susan Schwartz
Institute of Tectonics
1156 High Street
Santa Cruz, CA 95064

Secretary of the Air Force
(SAFRID)
Washington, DC 20330

Office of the Secretary of Defense
DDR&E
Washington, DC 20330

Thomas J. Sereno, Jr.
Science Application Int'l Corp.
10260 Campus Point Drive
San Diego, CA 92121

Dr. Michael Shore
Defense Nuclear Agency/SPSS
6801 Telegraph Road
Alexandria, VA 22310

Dr. Robert Shumway
University of California Davis
Division of Statistics
Davis, CA 95616

Dr. Matthew Sibol
Virginia Tech
Seismological Observatory
4044 Derring Hall
Blacksburg, VA 24061-0420

Prof. David G. Simpson
IRIS, Inc.
1616 North Fort Myer Drive
Suite 1440
Arlington, VA 22209

Donald L. Springer
Lawrence Livermore National Laboratory
L-025
P.O. Box 808
Livermore, CA 94550

Dr. Jeffrey Stevens
S-CUBED
A Division of Maxwell Laboratory
P.O. Box 1620
La Jolla, CA 92038-1620

Lt. Col. Jim Stobie
ATTN: AFOSR/NL
Bolling AFB
Washington, DC 20332-6448

Prof. Brian Stump
Institute for the Study of Earth & Man
Geophysical Laboratory
Southern Methodist University
Dallas, TX 75275

Prof. Jeremiah Sullivan
University of Illinois at Urbana-Champaign
Department of Physics
1110 West Green Street
Urbana, IL 61801

Prof. L. Sykes
Lamont-Doherty Geological Observatory
of Columbia University
Palisades, NY 10964

Dr. David Taylor
ENSCO, Inc.
445 Pineda Court
Melbourne, FL 32940

Dr. Steven R. Taylor
Los Alamos National Laboratory
P.O. Box 1663
Mail Stop C335
Los Alamos, NM 87545

Prof. Clifford Thurber
University of Wisconsin-Madison
Department of Geology & Geophysics
1215 West Dayton Street
Madison, WI 53706

Prof. M. Nafi Toksoz
Earth Resources Lab
Massachusetts Institute of Technology
42 Carleton Street
Cambridge, MA 02142

Dr. Larry Turnbull
CIA-OSWR/NED
Washington, DC 20505

Dr. Gregory van der Vink
IRIS, Inc.
1616 North Fort Myer Drive
Suite 1050
Arlington, VA 22209

Dr. Karl Veith
EG&G
5211 Auth Road
Suite 240
Suitland, MD 20746

Prof. Terry C. Wallace
Department of Geosciences
Building #77
University of Arizona
Tucson, AZ 85721

Dr. Thomas Weaver
Los Alamos National Laboratory
P.O. Box 1663
Mail Stop C335
Los Alamos, NM 87545

Dr. William Wortman
Mission Research Corporation
8560 Cinderbed Road
Suite 700
Newington, VA 22122

Prof. Francis T. Wu
Department of Geological Sciences
State University of New York
at Binghamton
Vestal, NY 13901

AFTAC/CA
(STINFO)
Patrick AFB, FL 32925-6001

DARPA/PM
3701 North Fairfax Drive
Arlington, VA 22203-1714

DARPA/RMO/RETRIEVAL
3701 North Fairfax Drive
Arlington, VA 22203-1714

DARPA/RMO/SECURITY OFFICE
3701 North Fairfax Drive
Arlington, VA 22203-1714

IRQ DNA
ATTN: Technical Library
Washington, DC 20305

Defense Intelligence Agency
Directorate for Scientific & Technical Intelligence
ATTN: DTIB
Washington, DC 20340-6158

Defense Technical Information Center
Cameron Station
Alexandria, VA 22314 (2 Copies)

TACTEC
Battelle Memorial Institute
505 King Avenue
Columbus, OH 43201 (Final Report)

Phillips Laboratory
ATTN: XPG
Hanscom AFB, MA 01731-5000

Phillips Laboratory
ATTN: GPE
Hanscom AFB, MA 01731-5000

Phillips Laboratory
ATTN: TSML
Hanscom AFB, MA 01731-5000

Phillips Laboratory
ATTN: SUL
Kirtland, NM 87117 (2 copies)

Dr. Svein Mykkeltveit
NTNT/NORSAR
P.O. Box 51
N-2007 Kjeller, NORWAY (3 Copies)

Dr. Michel Bouchon
I.R.I.G.M.-B.P. 68
38402 St. Martin D'Heres
Cedex, FRANCE

Prof. Keith Priestley
University of Cambridge
Bullard Labs, Dept. of Earth Sciences
Madingley Rise, Madingley Road
Cambridge CB3 0EZ, ENGLAND

Dr. Michel Campillo
Observatoire de Grenoble
I.R.I.G.M.-B.P. 53
38041 Grenoble, FRANCE

Dr. Jorg Schlittenhardt
Federal Institute for Geosciences & Nat'l Res.
Postfach 510153
D-3000 Hannover 51, GERMANY

Dr. Kin Yip Chun
Geophysics Division
Physics Department
University of Toronto
Ontario, CANADA

Dr. Johannes Schweitzer
Institute of Geophysics
Ruhr University/Bochum
P.O. Box 1102148
4360 Bochum 1, GERMANY

Prof. Hans-Peter Harjes
Institute for Geophysics
Ruhr University/Bochum
P.O. Box 102148
4630 Bochum 1, GERMANY

Trust & Verify
VERTIC
8 John Adam Street
LONDON WC2N 6EZ, ENGLAND

Prof. Eystein Husebye
NTNF/NORSAR
P.O. Box 51
N-2007 Kjeller, NORWAY

David Jepsen
Acting Head, Nuclear Monitoring Section
Bureau of Mineral Resources
Geology and Geophysics
G.P.O. Box 378, Canberra, AUSTRALIA

Ms. Eva Johannisson
Senior Research Officer
FOA
S-172 90 Sundbyberg, SWEDEN

Dr. Peter Marshall
Procurement Executive
Ministry of Defense
Blacknest, Brimpton
Reading RG7-FRS, UNITED KINGDOM

Dr. Bernard Massinon, Dr. Pierre Mechler
Societe Radiomana
27 rue Claude Bernard
75005 Paris, FRANCE (2 Copies)